Decoding Movement-Related Cortical Potentials Based on Subject-Dependent and Section-Wise Spectral Filtering

Ji-Hoon Jeong, No-Sang Kwak, Cuntai Guan, *Fellow, IEEE,* and Seong-Whan Lee, *Fellow, IEEE*

***Abstract*— An important challenge in developing a movement-related cortical potential (MRCP)-based brain-machine interface (BMI) is an accurate decoding of the user intention for real-world environments. However, the performance remains insufficient for real-time decoding owing to the endogenous signal characteristics compared to other BMI paradigms. This study aims to enhance the MRCP decoding performance from the perspective of preprocessing techniques (i.e., spectral filtering). To the best of our knowledge, existing MRCP studies have used spectral filters with a fixed frequency bandwidth for all subjects. Hence, we propose a subject-dependent and section-wise spectral filtering (SSSF) method that considers the subjects' individual MRCP characteristics for two different temporal sections. In this study, MRCP data were acquired under a powered exoskeleton environments in which the subjects conducted self-initiated walking. We evaluated our method using both our experimental data and a public dataset (BNCI Horizon 2020). The decoding performance using the SSSF was 0.86 (±0.09), and the performance on the public dataset was 0.73 (±0.06) across all subjects. The experimental results showed a statistically significant enhancement (p<0.01) compared with the fixed frequency bands used in previous methods on both datasets. In addition, we presented successful decoding results from a pseudo-online analysis. Therefore, we demonstrated that the proposed SSSF method can involve more meaningful MRCP information than conventional methods.**

Manuscript received September 2, 2019; revised December 27, 2019; accepted January 5, 2020. Date of publication January 15, 2020; date of current version March 6, 2020. This work was supported in part by the Institute of Information & Communications Technology Planning & Evaluation (IITP) Grant funded by the Korea Government (Development of Non-Invasive Integrated BCI SW Platform to Control Home Appliances and External Devices by User's Thought via AR/VR Interface) under Grant 2017-0-00432 and in part by the Institute of Information & Communications Technology Planning & Evaluation (IITP) Grant funded by the Korea Government (Development of BCI based Brain and Cognitive Computing Technology for Recognizing User's Intentions using Deep Learning under Grant 2017-0-00451. *(Ji-Hoon Jeong and No-Sang Kwak contributed equally to this work.) (Corresponding author: Seong-Whan Lee.)*

Ji-Hoon Jeong and No-Sang Kwak are with the Department of Brain and Cognitive Engineering, Korea University, Seoul 02841, South Korea (e-mail: jh_jeong@korea.ac.kr; nskwak@korea.ac.kr).

Cuntai Guan is with the School of Computer Science and Engineering, Nanyang Technological University, Singapore 639798 (e-mail: ctguan@ntu.edu.sg).

Seong-Whan Lee is with the Department of Artificial Intelligence, Korea University, Seoul 02841, South Korea, and also with the Department of Brain and Cognitive Engineering, Korea University, Seoul 02841, South Korea (e-mail: sw.lee@korea.ac.kr).

This article has supplementary downloadable material available at http://ieeexplore.ieee.org, provided by the authors.

Digital Object Identifier 10.1109/TNSRE.2020.2966826

***Index Terms*— Brain-machine interface, electroencephalography, movement-related cortical potentials.**

I. Introduction

BRAIN-MACHINE interfaces (BMIs) are communication systems that provide a bridge between users and external devices. BMIs convey the user's intention without direct manipulation or activation of the peripheral nervous system [1]–[4]. The BMI technique commonly employs electroencephalography (EEG) signals to recognize user intentions for controlling external devices, such as a wheelchair [5], [6], a robotic arm [7]–[10], or a powered exoskeleton [11]–[14]. EEG-based BMI technologies have been developed for patients with paralysis or nerve damage (for example, spinal cord injury or stroke) for neuro-rehabilitation, as well as for healthy individuals [15]–[20]. An important factor of a natural BMI system is the voluntary intention of users to conduct various movements, such as walking, ankle dorsiflexion, arm flexion/extension, or hand grasping [21]–[27].

The neural correlates of a movement intention from EEG signals can be represented as an event-related desynchronization and synchronization (ERD/ERS) and a movement-related cortical potential (MRCP) [28]–[32]. In particular, an MRCP is a spontaneous potential generated by the execution/imagination of a self-initiated movement paradigm or cue-based movement paradigm, which is known to be contingent negative variation (CNV). An MRCP comprises two main components: a readiness potential (RP) and a movement-monitoring potential (MMP) [33], [34]. The RP is a negative cortical potential, which begins approximately 1∼2 s before the onset of a voluntary movement activated over the pre-supplementary motor area (pre-SMA) or the contralateral primary motor cortex (M1). An MMP is a slow positive deflection associated with the outcome of the motor process after the execution of the movement intention over M1. Therefore, owing to its characteristics such as a potential spontaneity and early detection of user intentions, an MRCP decodes the process of movement preparation/execution based on a single-trial basis. Hence, this potential can be mostly used for BMI-based neuro-rehabilitation for patients utilizing the assistive devices [14], [35].

Conventional BMI studies have shown that various functional movements can be decoded using MRCP, such as voluntary arm movements [8], [23], [36]–[38], sitting and

standing transitions [39], finger movements (pressing a button) [40], [41], executed and imagined foot movements [30], [42]–[44], and self-initiated walking [17], [45], [46]. Various signal processing methods have been adopted, including different types of spatial [44] and spectral filters (e.g., an infinite impulse response (IIR) [37], [42] or a finite impulse response (FIR) filters [47], [48]), along with the creation of an MRCP template for matching [49], the modification of a conventional classifier [39], [43], [50], [51], the adoption of an artifact rejection method [52], the proposal of feature combination methods [46], [53], [54], and the use of different preprocessing methods [55]–[57]. In addition, a few groups have investigated the ability to extend an MRCP-based BMI to real-time environments [42], [58].

Single-trial based MRCP decoding is needed for BMI users to control external devices reliably and efficiently. Therefore, an improvement in the MRCP decoding performance with a low latency for a single-trial is one of the challenging BMI issues. To solve these limitations, various signal processing methods and paradigms have been proposed [34], [59]. In this study, we hypothesized that 1) using subject-dependent MRCP features and 2) applying separate spectral bands to the RP and MMP sections can improve the MRCP decoding performance. Note that previous studies have only used a static spectral band in the entire MRCP temporal section for signal preprocessing [37], [42], [43], [50].

Hence, our main contributions are three-fold: 1) We propose a subject-dependent and section-wise spectral filtering (SSSF) method based on machine learning that can accurately determine a user's intention on a single-trial basis. 2) We demonstrate the usefulness of the proposed method using both our experimental data (i.e., lower limb MRCP) and the public dataset of BNCI Horizon 2020 (i.e., upper limb MRCP) [50]. Finally, 3) we present successful decoding accuracies from an offline analysis and a pseudo-online analysis.

II. Materials and Methods

A. Participants

Ten healthy subjects (S1-S10; 10 males; 20-30 years in age) participated in the experiment. All subjects were healthy without any known neurophysiological anomalies or musculoskeletal disorders. The experimental environments and protocols were reviewed and approved by the Institutional Review Board at Korea University (1040548-KU-IRB-17-181-A-2). All subjects gave their informed consent according to the Declaration of Helsinki prior to the experiment.

B. Experimental Protocols

We designed the experimental environments for acquiring MRCP data using a powered exoskeleton to reflect similar environments for neuro-rehabilitation and for real-world BMI scenarios. The experiment setup was composed of three main modules (Fig. 1).

1) A Powered Exoskeleton Module: We used the lower limb exoskeleton (Rex, Rex Bionics, New Zealand) for gait assistance. The exoskeleton can support itself and the weight of the user, as well as programmed motions that perform essential functions such as walking, turning, sitting, and standing. In our experiment, we used the walking forward and standing functions of the exoskeleton.

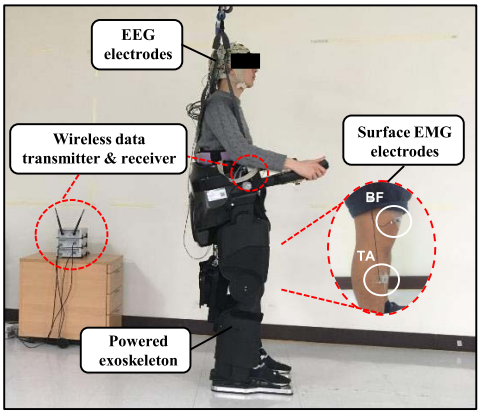

Fig. 1. Experiment setup and protocols for MRCP data on exoskeleton walking. The experiment environments comprised two EMG electrodes, a wireless data transmitter and receiver, and the powered exoskeleton.

2) EEG Module: A wireless EEG interface (MOVE System, BrainProduct GmbH, Germany) was used to acquire EEG signals under an ambulatory environment. The EEG signals were acquired using an active-electrode system (ActiCAP Systems, Brain Products GmbH, Germany) with 32 channels. EEG signals were transmitted to the recording device. The wireless device was located on the right arm of the exoskeleton and was firmly fixed such that it was not disturbed by the exoskeleton movement. The wireless data receiver and signal amplifiers were connected to the EEG cap through a wireless interface.

3) EMG Module: The surface electromyography (EMG) module acquired electrical signals from muscle activation of the right leg to control the exoskeleton walking. The EMG signals were recorded using the data transfer device and amplifier with two bipolar Ag/AgCl electrodes on the tibialis anterior (TA) and biceps femoris (BF) muscles of the right leg; note that these muscles are known as fast activation muscles for walking [46]. Movement onset triggers were marked when the EMG activity exceeded a pre-defined threshold value. The exoskeleton executed the walking function when trigger information associated with muscle activation was received.

C. Data Acquisition

Scalp EEG and surface EMG signals were, simultaneously, recorded during the experiment. The EEG signals were acquired using 32 channels placed at Fp1, Fz, F3, F7, C1, FC5, FC1, C3, T7, CPz, CP5, CP1, Pz, P3, P7, O1, Oz, O2, P4, P8, CP6, CP2, Cz, C4, T8, C2, FC6, FC2, F4, F8, Fp2, and POz. The ground and reference electrodes were placed at FPz and FCz, respectively. The electrodes were positioned according to the 10/20 international system. The impedance of the electrodes was maintained at below 10 kΩ throughout the experiment. The EEG signals were digitized at a sampling frequency of 1,000 Hz. The notch filter frequency rate was set at 60 Hz to reduce the DC power supply noise.

EMG signals were recorded to transfer the trigger information in real-time for exoskeleton control. The impedance of the EMG electrodes was maintained at below 20 kΩ during the experiment, and the data were preprocessed using a 2 s sliding window with a 100 ms shift and were bandpass filtered from 100–125 Hz with a Butterworth second-order zero-phase shift bandpass filter [46]. The data were rectified using the absolute value, and we calculated the moving average of EMG amplitudes in the window size. The movement onset was marked when the value of moving average exceeded the pre-defined threshold determined based on a simple threshold criterion [60] across each subject.

D. Experimental Paradigm

The subjects wearing exoskeleton were instructed to perform self-initiated walking after an intending walk (Fig. 2). The experiment was conducted for a total of 50 trials. Each trial was composed of three states: resting, walking intention, and exoskeleton walking (self-initiated). During a resting state, the subjects were instructed to not perform any tasks. They relaxed their muscle after each trial within 10 s because EMG contamination owing to muscle tension can impede the detection of the movement onset. After resting, the subjects attempted to move their right leg as if they were starting to walk. At this point, our experimental system detected the movement onset trigger generated from the EMG activation of the right leg (intention state). Then, upon self-initiated exoskeleton walking, the exoskeleton executed walking function as a half-gait cycle for more than 10 s.

E. EEG Pre-Processing

The EEG data analysis was conducted using the BBCI [61] and OpenBMI [62] toolbox under a MATLAB 2018b environment. We used interpolation and an antialiasing filter [63], [64] to down-sample the acquired EEG data from 1,000 to 100 Hz to consider the continuous BMI decoding for real-world scenarios. The EEG channels with respect to eye blinks and facial/cranial muscle activity were removed (e.g., Fp−, F−, T−, O−, P−, PO−) to reject artifacts [39]. In addition, the data were re-referenced using a large Laplacian spatial filter to compensate for the poor spatial resolution of scalp EEG recordings [42], [49], [65]. The spatial filter was applied to the C1, C2, CPz, and Cz channels with eight surrogate channels, and these four channels were finally selected for a data analysis.

F. SSSF

The preprocessed EEG data were segmented into 6 s epochs (−5 to 1 s) based on movement onset triggers (0 s) for offline analysis. During the 6 s epochs, EEG data from −2 to 1 s were defined as the "walking intention" class (MRCP activation), and the remaining data from −5 to −2 s were defined as the "resting" class. The data from each class were composed of the time × channel × trial (300 × 4 × 50). The data for the walking intention class were then separated into RP (−2 to 0 s) and MMP (0 to 1 s) temporal sections to consider each MRCP component characteristic.

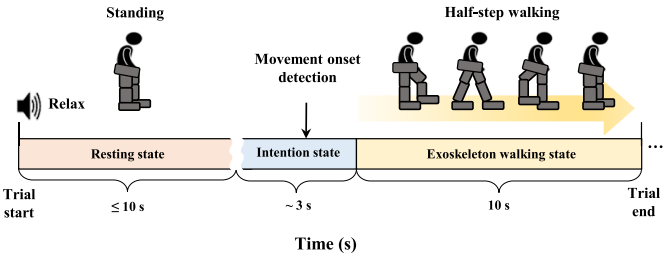

Fig. 2. The experiment paradigm consisted of three states: a resting state of approximately 10 s, an intention state, and 10 s exoskeleton walking. When the subjects intended a self-initiated walking, the EMG signals were over the pre-defined threshold. Based on the threshold, the exoskeleton applied the half-step walking.

We then composed the frequency filter bank (S) to select the spectral bands according to each temporal section with the best performance. The frequency filter bank comprises 30 different spectral bands related to the MRCP activation, which consists of lower cutoff frequencies (0.05, 0.1, and 0.5 Hz) and upper cutoff frequencies (1, 2, 3, …, and 10 Hz). We applied a spectral filter to each temporal section using a FIR filter with a zero-phase, 50^{th} order Hamming window. In this study, we adopted the FIR filter to consider short-length EEG data, such as a 3 s sliding window.

To extract the MRCP features, during the training phase, we calculated the mean amplitude feature vector in 0.2 s intervals from each RP and MMP section. Hence, we obtained each feature matrix (channels × feature vectors) from the RP and the MMP sections. Consequently, each RP and MMP feature was concatenated with MRCP features to consider all combinations of each spectral band.

A binary regularized linear discriminant analysis (RLDA) classifier, which is a robust classification method that uses a normal distribution in each class sample [66], [67], was used to discriminate between the walking intention and the resting classes. The classifier was trained to reduce the dimensionality of the data toward a feature vector space and to classify samples into either group, related to each class. We selected two spectral bands (Sb_{RP} for RP section and Sb_{MMP} for MMP section) with the best decoding performance according to the $k \times j$ classification accuracies ($ACC_{k,j}$) using the validation dataset. A 5-fold cross-validation was used for a fair validation to select the optimal spectral bands.

During the test phase, we separated the new single-trial EEG data into two sections using the same method applied during the training phase. We then applied spectral filtering for each section with the selected spectral bands ($B_{selected}$). After combining the mean amplitude features, the RLDA classifier selected in the training phase was finally used to classify the walking intention and resting for the test data. The proposed SSSF is shown in Fig. 3 and Algorithm 1.

In addition, the proposed SSSF was designed for an asynchronous MRCP detection. Throughout the offline analysis, the data of each class including 50 trials were used to train and validate the SSSF. In this study, for the pseudo-online analysis, the time parameter of the epoch data was modified from a 6 s to 3 s epoch such that we adopted the 3 s epoch data as a window to consider the latency of the

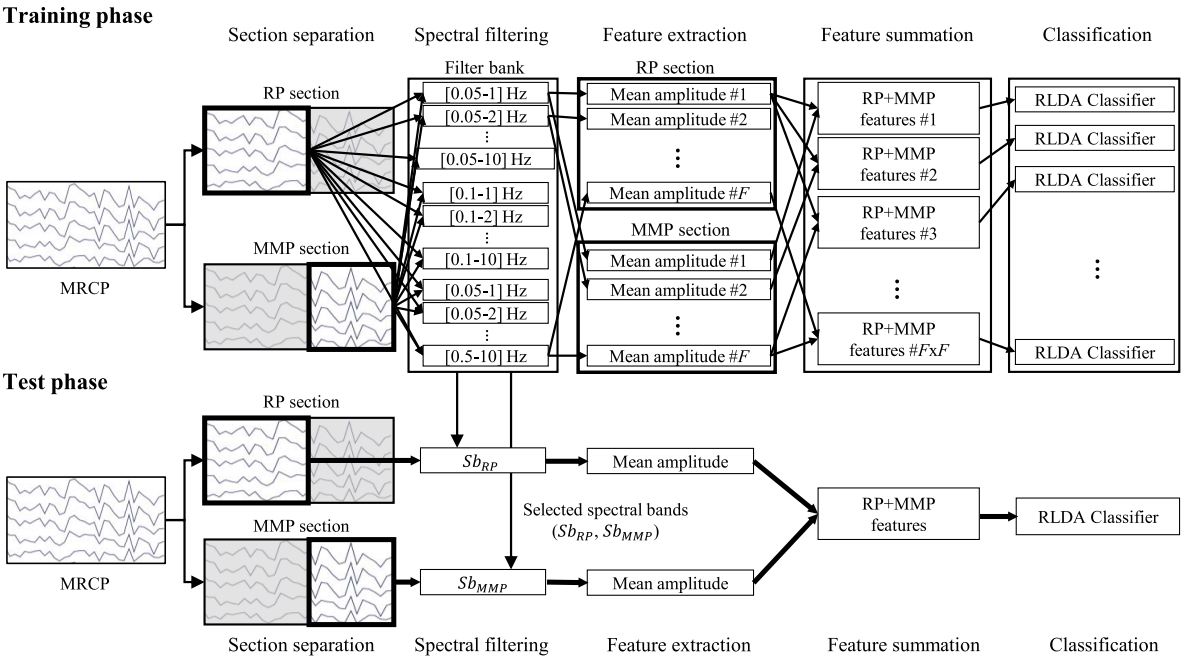

Fig. 3. Overall flowchart for MRCP decoding based on the proposed SSSF method.

continuous decoding. Each 3 s epoch window could detect the subject's walking intention using a pre-trained SSSF during a single-trial.

G. Performance Evaluation for Our Experiment

1) Offline Analysis: To evaluate the proposed SSSF method, we compared it with existing spectral filtering methods during an offline analysis. First, we randomly selected 50% of the trials from all data for training and validation and used the remaining 50% of trials for the testing. Using the test data, the decoding performance was evaluated across each subject. Note that we evaluated the classification performance between the walking intention and resting state across all trials.

2) Pseudo-Online Analysis: We also evaluated the proposed method through a pseudo-online analysis [68], [69] to confirm the feasibility of real-world MRCP-based BMI scenarios. We adopted a fully automated online artifact removal method for brain-computer interfacing (FORCe), which can apply thresholding to reject very high amplitude characteristics, to remove noise related to the body and head movements from the EEG data [70]. The EEG data were evaluated with a sliding window of 3 s applied to the time interval (−4 to 4 s) with a sliding overlap of 0.05 s. Each window was also processed with the same spectral filtering and classifier parameters used during the training phase of the offline analysis. The labels of walking class were pre-assigned in the −2 to 1 s time intervals based on the movement onset mark (0 s). The other labels were defined as the resting class. Therefore, the classified values of each window were evaluated for each trial between the pre-assigned true labels and the decoded results.

H. Performance Evaluation for Public Dataset

In addition, we validated the SSSF on the public EEG dataset, published through the BNCI Horizon 2020 project, which contains various upper extremity tasks, such as an elbow flexion/extension, wrist supination/pronation, hand open/close, and resting [50]. Fifteen subjects participated in the experiment (6 males and 9 females, 22-40 years in age). The dataset comprised EEG data from 61 channels with a 512 Hz sampling rate. To evaluate the SSSF on the dataset, we randomly divided the data into a training set and a test set at a 50:50 ratio. The EEG data were preprocessed using the same steps as those applied in the offline analysis to apply the proposed SSSF (e.g., spatial filtering, time segmentation, and binary class selection). We evaluated the MRCP decoding performance between each class and the resting class to prove the availability of the SSSF.

TABLE I
DECODING PERFORMANCES WITH THE SELECTED SPECTRAL BANDS ACROSS EACH SUBJECT USING THE TEST DATASET

Subjects	Selected spectral bands [Hz]		Decoding performances
	RP section	MMP section	
S1	[0.1–4]	[0.05–6]	0.96
S2	[0.5–7]	[0.05–8]	0.74
S3	[0.5–1]	[0.1–3]	0.70
S4	[0.1–1]	[0.05–7]	0.86
S5	[0.05–2]	[0.05–3]	0.94
S6	[0.1–10]	[0.5–5]	0.74
S7	[0.5–3]	[0.1–5]	0.96
S8	[0.5–4]	[0.05–3]	0.86
S9	[0.05–1]	[0.05–10]	0.90
S10	[0.1–1]	[0.5–5]	0.94
Average			**0.86 (±0.09)**

III. RESULTS

Table I shows the selected spectral bands for RP and MMP temporal sections and the corresponding performance according to each subject. The selected spectral bands had different

Algorithm 1 SSSF

Input: MRCP data $\{X, Y, \Omega\}$ and frequency filter bank S

- $X = \{x_i\}_{i=1}^{D}$, $\{x_i\} \in \mathbb{R}^{N \times T}$: a set of single-trial EEG data for RP section, where D is the total number of trials with N channels and T sample points
- $Y = \{y_i\}_{i=1}^{D}$, $\{y_i\} \in \mathbb{R}^{N \times T}$: a set of single-trial EEG data for MMP section, where D is the total number of trials with N channels and T sample points
- $\Omega = \{O_i\}_{i=1}^{D}$: corresponding class labels, where $O_i \in \{1, 0\}$ and D is the total number of trials
- $S = \{S_i\}_{i=1}^{F}$: frequency filter bank comprising spectral bands S_i where i^{th} is spectral bands and F is the total number of bands

Output: Selected spectral bands of each RP and MMP section

- $B_{selected} = \{Sb_{RP}, Sb_{MMP}\}$

for $k = 1$ ***to*** F **do**
  $RP_k = S_k \otimes X$ ▷ $\otimes$: Band pass filtering
  ▷ RP_k: Filtered data using k^{th} spectral band
  for $j = 1$ ***to*** F **do**
    $MMP_j = S_j \otimes Y$ ▷ MMP_j: Filtered data using j^{th} spectral band
    Divide the filtered data RP_k, MMP_j into H subsets ▷ $\{RP_k\}$: $\{RP_{k,1}, RP_{k,2}, \ldots RP_{k,H}\}$
    ▷ $\{MMP_j\}$: $\{MMP_{j,1}, MMP_{j,2}, \ldots MMP_{j,H}\}$
    ▷ H: the total number of fold for cross-validation
    for $h = 1$ ***to*** H **do**
      $RP\_tr_h = \{RP_k\}\text{-}\{RP_{k,h}\}$ ▷ RP_tr_h: Training data for RP section
      $RP\_val_h = \{RP_{k,h}\}$ ▷ RP_val_h: Validation data for RP section
      $MMP\_tr_h = \{MMP_j\}\text{-}\{MMP_{j,h}\}$ ▷ MMP_tr_h: Training data for MMP section
      $MMP\_val_h = \{MMP_{j,h}\}$ ▷ MMP_val_h: Validation data for MMP section
      for $i = 1$ ***to*** $\frac{H-1}{H} \times D$ **do**
        $F\_tr_h = f\_tr_h^i$ ▷ $f\_tr_h^i$: *Concatenate*(Mean amplitude of $RP\_tr_h^i$, Mean amplitude of $MMP\_tr_h^i$)
      end
      for $i = 1$ ***to*** $\frac{D}{H}$ **do**
        $F\_val_h = f\_val_h^i$ ▷ $f\_val_h^i$: *Concatenate*(Mean amplitude of $RP\_val_h^i$, Mean amplitude of $MMP\_val_h^i$)
      end
      $(w_h, b_h) = RLDA(F\_tr_h, \Omega\_tr_h)$ ▷ Train a RLDA classifier, Ω_tr_h: $\{O_i\}_{i=1}^{\frac{H-1}{H} \times D}$
      $Y_h = (w_h)^T \cdot F\_val_h + b_h$ ▷ Evaluate the validation data using trained classifier parameters
      $P_h = \begin{cases} 1 & if,\ Y_h \geq 0 \\ 0 & otherwise \end{cases}$
      $\theta_h = 1\text{-}\ error(P_h, \Omega\_val_h)$ ▷ Performance evaluation, Ω_val_h: $\{O_i\}_{i=1}^{\frac{D}{H}}$
    end
    $ACC_{k,j} = \frac{1}{H} \sum_{h=1}^{H} \theta_h$ ▷ Calculate averaged decoding performances for H-fold cross-validation
  end
end
$\{idx\_k, idx\_j\} = argmax_{k,j}(ACC_{k,j})$ ▷ Find the values of k and j when the ACC is the best performance
$Sb_{RP} = S_{idx\_k}$, $Sb_{MMP} = S_{idx\_j}$ ▷ Sb_{RP} and Sb_{MMP}: Selected spectral bands for RP and MMP sections
$B_{selected} = \{Sb_{RP}, Sb_{MMP}\}$

bandwidth for the RP and MMP sections and were distinct across each subject. The grand-average decoding performance was 0.86 (±0.09) across all subjects.

Table II compares the decoding performance between the SSSF and heuristic spectral filtering, which is used in most conventional studies, such as 0.05–5 Hz [37], 0.05–10 Hz [43], 0.1–1 Hz [42], and 0.3–3 Hz [50] for MRCP decoding. The results showed that the proposed SSSF produced the best grand-average decoding performance across all subjects. The averaged decoding performances for each spectral band were 0.78 (±0.13) at 0.05–5 Hz, 0.78 (±0.13) at 0.05–10 Hz, 0.72 (±0.10) at 0.1–1 Hz, and 0.77 (±0.13) at 0.1–4 Hz. In particular, subject S1, who had the best performance, showed the same results in the comparative groups (0.05–5 Hz, 0.05–10 Hz, and 0.3–3 Hz). According to these results, the proposed SSSF is more effective for subjects with a relatively low MRCP decoding performance.

Table III compares the decoding performance between using multi-channels and a single-channel. The Cz, C1, C2, and CPz were selected as multiple channels, and the Cz channel alone was selected as the single-channel, which can

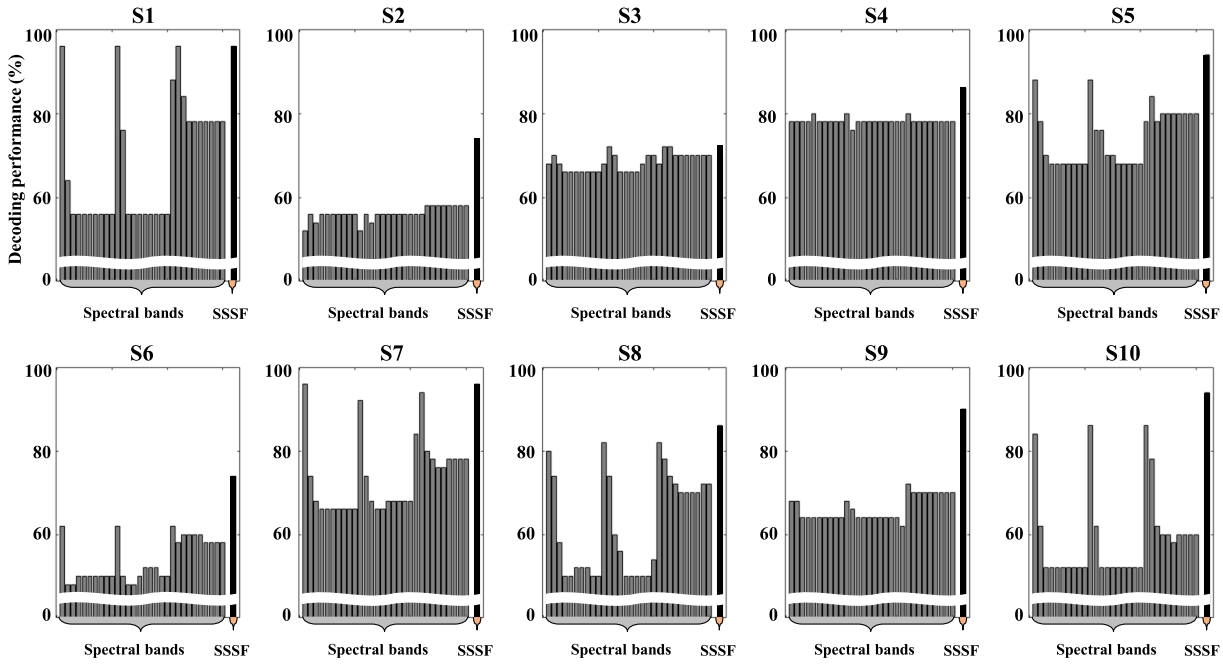

Fig. 4. Comparison of the decoding performances among the proposed method and the assigned spectral bands (e.g., 0.05–1 Hz, …, 0.5–10 Hz) across each subject. The gray and black bars indicate the decoding performances using only static spectral bands of the entire temporal section (−2 to 1 s) and the proposed SSSF, respectively.

TABLE II
COMPARISON OF THE DECODING PERFORMANCE USING THE FIXED- AND SUBJECT-DEPENDENT SPECTRAL BANDS

Subjects	Decoding performances				
	0.05–5 Hz [37]	0.05–10 Hz [43]	0.1–1 Hz [42]	0.3–3 Hz [50]	SSSF
S1	0.96	0.96	0.82	0.96	0.96
S2	0.58	0.56	0.54	0.56	0.74
S3	0.70	0.70	0.68	0.70	0.70
S4	0.78	0.78	0.78	0.78	0.86
S5	0.92	0.90	0.80	0.88	0.94
S6	0.64	0.64	0.64	0.64	0.74
S7	0.94	0.94	0.84	0.88	0.96
S8	0.78	0.82	0.80	0.84	0.86
S9	0.70	0.70	0.60	0.66	0.90
S10	0.84	0.84	0.78	0.88	0.94
Average	**0.78 (±0.13)**	**0.78 (±0.13)**	**0.72 (±0.10)**	**0.77 (±0.13)**	**0.86 (±0.09)**

TABLE III
COMPARISON OF DECODING PERFORMANCES BETWEEN MULTIPLE CHANNELS AND A SINGLE-CHANNEL USING THE SSSF

Subjects	Decoding performances	
	Multi-channels (Cz, C1, C2, and CPz)	Single-channel (Cz)
S1	0.96	0.96
S2	0.74	0.70
S3	0.70	0.68
S4	0.86	0.80
S5	0.94	0.94
S6	0.74	0.62
S7	0.96	0.96
S8	0.86	0.90
S9	0.90	0.70
S10	0.94	0.90
Average	**0.86 (±0.09)**	**0.81 (±0.13)**

represent the prominent MRCP patterns among all of the EEG channels. The selected Cz as a single-channel has been reported as a dominant channel owing to the observation of brain modulations concerning the lower-limb movement (e.g., walking and foot dorsiflexion) in the motor cortical region [34], [63]. This processing was consistent with the experimental protocols and analysis reported in [42], [51], and [52]. The results showed that the grand-average decoding performances were 0.86 (±0.09) for the multiple channels and 0.81 (±0.13) for the single-channel across all subjects. The decoding performance tends to decrease by approximately 5% when using only the Cz channel. However, subjects S1, S5, and S7, who showed a high accuracy, did not exhibit differences between single and multiple channels.

Fig. 4 shows the decoding performances using the single spectral filtering method in the entire MRCP activation section (−2 to 1 s) for 30 different spectral bands, such as 0.05–1 Hz, 0.05–2 Hz, …, 0.05–10 Hz, 0.1–1 Hz, 0.1–2 Hz, …, 0.1–10 Hz, 0.5–1 Hz, 0.5–2 Hz, …, and 0.5–10 Hz. Most subjects showed a higher performance when using the proposed SSSF than when using single spectral filtering for the entire section. Indeed, the SSSF method showed an increase in performance of approximately 7% compared with the best accuracy of the single spectral filtering method. Subjects S1 and S7 showed the highest decoding performance (0.96) but the same performance was shown when using the SSSF a single spectral filter.

Fig. 5 shows that the MRCP exhibits a negative and a positive amplitude deflection from −2 to 1 s for S4 and S10 as the representative subjects. The actual movement onset (0 s) was

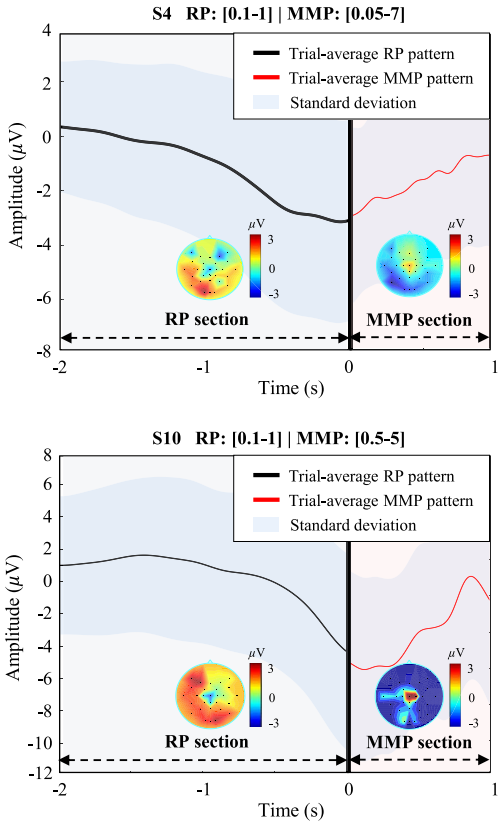

Fig. 5. Time-amplitude representation of the trial-average RP and MMP patterns in channel Cz in subjects S4 and S10. The scalp maps showed the spatial representation according to each RP and MMP section.

set when the EMG signals exceeded a pre-defined threshold amplitude. The black and red lines denote the trial-average RP and MMP patterns in the Cz channel, respectively. Each RP and MMP pattern adopting the selected spectral filtering showed negative shapes before the onset of movement (RP section) and represented positive waves in the MMP section. The blue area denotes the standard deviation of the RP and MMP amplitudes according to each trial. Scalp topographies are plotted to show the spatial pattern distribution for each RP and MMP section. The topographies represent the average amplitude across all trials during each time interval for the representative subjects. The time interval is separated into two sections to observe the brain dynamics during a movement intention. Before the initiation of walking (−2 to 0 s), the brain activity showed a gradually negative distribution near the motor cortex, such as at Cz, C1, and C2 channels. After movement onset in the MMP section (0 to 1 s), the intensity of the spatial distribution returned from a negative to positive spatial distribution.

Fig. 6 shows the decoding trends of the walking intention according to all spectral bands used during our experiment (x-axis for the MMP section and y-axis for the RP section). Each pixel represents the decoding accuracy using each spectral band. The pixels with the best classification accuracy are denoted with black square boxes. We confirmed that the proposed SSSF method selected different spectral bands for each subject-dependent and each MRCP component. It was demonstrated that applying the preprocessing method according to each subject and MRCP component has a greater effective than using the method in the same way across all subjects. Fig. 6 provides further details of this.

Fig. 7 shows the pseudo-online analysis results of our experiment data. Note that the total length of each trial used in the pseudo-online analysis was 8 s (−4 to 4 s). Similar to the offline analysis, we used a 3 s sliding window with an overlap of 0.05 s. Therefore, we acquired 100 classification results per trial. The black dashed line indicates the movement onset mark (0 s), and each gray box represents the walking class. For all subjects, most of the epochs around the movement onset were classified correctly. Subjects S1, S4, S5, S7, S8, and S10 showed relatively clear results for all trials compared with the other subjects. However, although we applied the artifact removal technique to prevent malfunctions of the movement artifacts, we were unable to avoid large misclassifications when the subjects walked.

Table IV shows the evaluation results of decoding the user intention using the proposed SSSF on the public dataset (BNCI Horizon 2020). We conducted an evaluation between one of the movement classes and the resting class. The grand-average results showed 0.74 (±0.07) for elbow flexion vs. rest, 0.73 (±0.08) for elbow extension vs. rest, 0.73 (±0.08) for supination vs. rest, 0.70 (±0.09) for pronation vs. rest, 0.72 (±0.09) for hand close vs. rest, and 0.76 (±0.06) for hand open vs. rest, respectively, across all subjects. In addition, we applied multi-class classification on all classes of movement and the resting class (seven classes in a total). The grand-average classification performance showed 0.38 (±0.15) across all subjects. The results showed higher results than the chance rate accuracy of approximately 0.14.

Table V compares the decoding performances between the conventional spectral filters and the proposed SSSF for the public dataset. The results were evaluated using the representative binary classification of the hand open class and the resting class. Decoding performances of 0.48 (±0.05) at 0.05–5 Hz, 0.51 (±0.02) at 0.05–10 Hz, 0.49 (±0.03) at 0.1–1 Hz, 0.50 (±0.09) at 0.3–3 Hz, and 0.76 (±0.06) for the proposed SSSF were obtained. We also confirmed that SSSF showed better results than a single frequency filtering method on the upper limb MRCP data.

For a statistical analysis of the decoding performance using our dataset and the public dataset, we adopted multiple comparisons through a Bonferroni correction. Initially, we validated the normality and homoskedasticity of each comparative group (e.g., 0.05–5 Hz versus SSSF in Table VI) owing to the small number of samples. The normality for each conventional method using the Shapiro–Wilk test was satisfied with a null hypothesis (H0), and the assumption of homoscedasticity based on Levene's test was also met for each comparative group. Hence, we could conduct a statistical analysis between the conventional method and the proposed SSSF using multiple comparisons with a Bonferroni correction. Table VI shows the p-value of each comparative group. The proposed SSSF versus other conventional methods showed significant differences ($p<0.01$) not only with our dataset but also with the public dataset. However, a comparison between

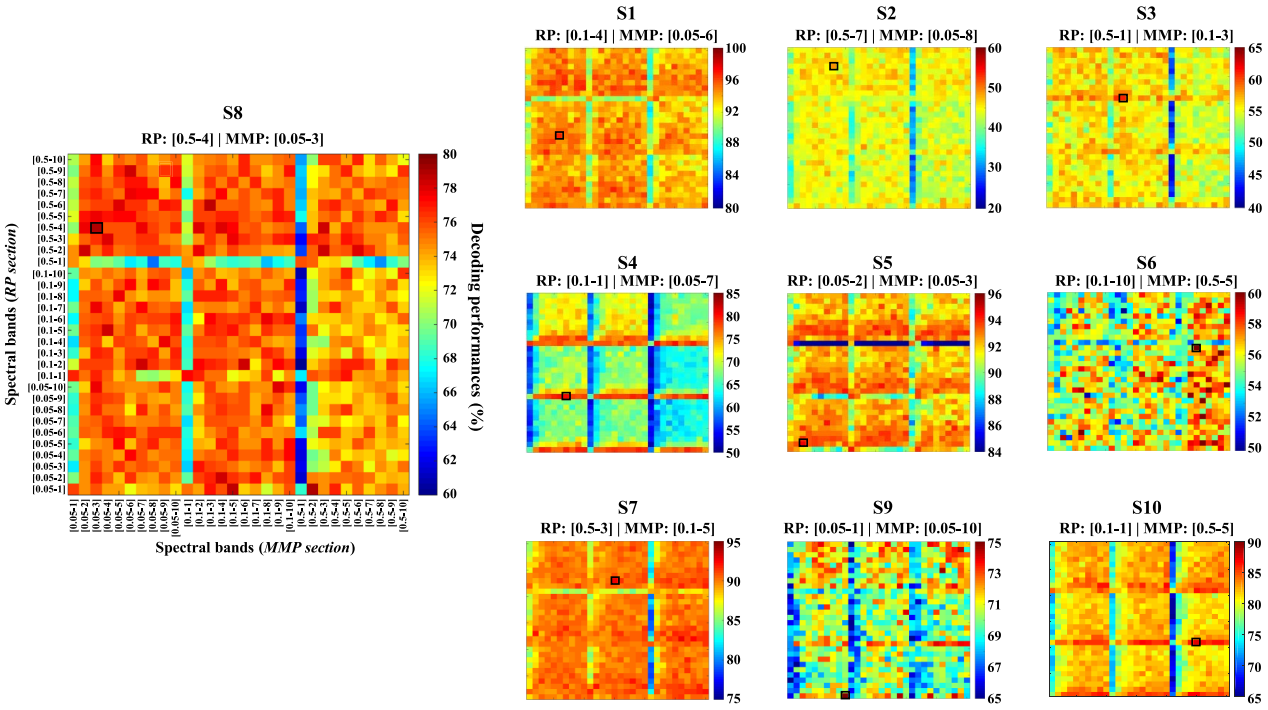

Fig. 6. Decoding trends across spectral bands for each RP and MMP section. Each pixel represents the decoding performance using different filter bands, which are selected during the training phase. The black square denotes the best performance.

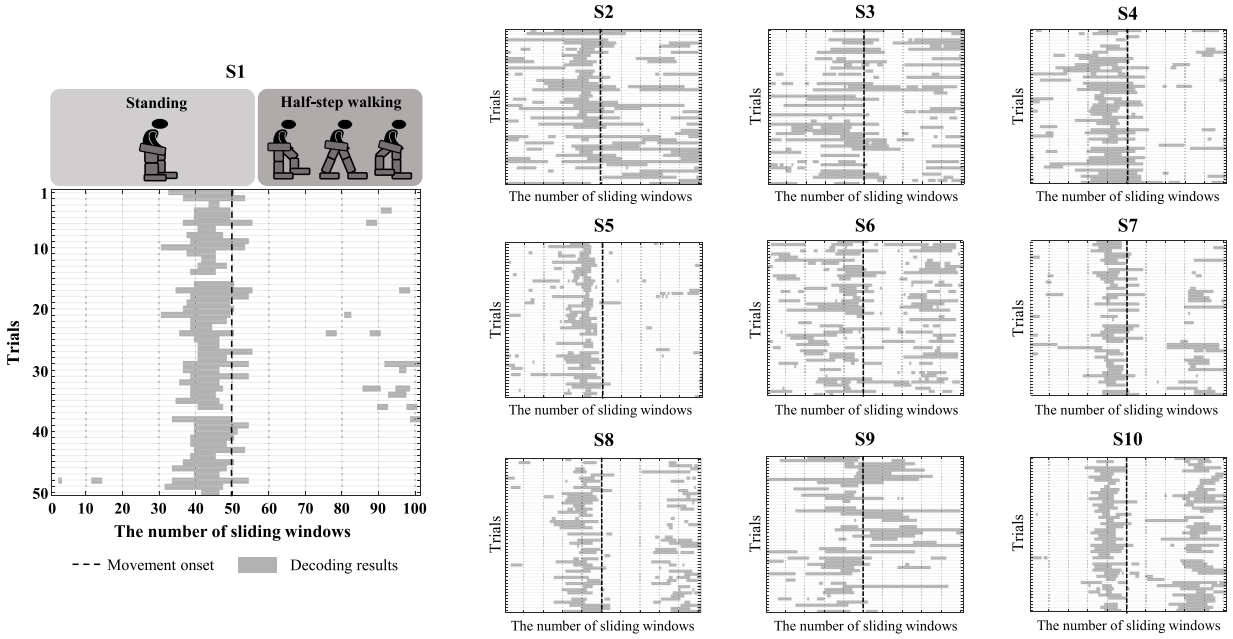

Fig. 7. Representation of the classification outputs in the pseudo-online analysis across each subject. The gray squares indicate the classification output for the walking intention class, and the white squares show the results for the resting state class.

conventional methods showed no significant interaction with a high p-value (>0.05).

IV. Discussion

In this study, we demonstrated the possibility of robust detection of user intentions from an MRCP when applying our experimental data and the public dataset. The experiment data were acquired from the MRCP data to detect the walking intention under a lower-limb exoskeleton environment. We proposed the use of SSSF method, an MRCP feature selection method that considers the individual characteristics of a subject's EEG signals through a pre-processing step. As a result, the SSSF showed the highest decoding performance compared to conventional methods for not only our experimental data but also the public dataset.

TABLE IV
EVALUATION RESULTS OF MRCP DECODING FOR THE PROPOSED SSSF USING PUBLIC MRCP DATA [50]

Subjects	Decoding performances						
	elbow flexion vs. rest	elbow extension vs. rest	supination vs. rest	pronation vs. rest	hand close vs. rest	hand open vs. rest	Multi-class (7-class)
S1	0.76	0.73	0.68	0.75	0.73	0.73	0.32
S2	0.69	0.75	0.81	0.76	0.65	0.80	0.45
S3	0.70	0.66	0.63	0.72	0.68	0.72	0.33
S4	0.82	0.72	0.79	0.77	0.70	0.76	0.54
S5	0.68	0.68	0.80	0.78	0.76	0.81	0.42
S6	0.78	0.81	0.88	0.85	0.80	0.75	0.65
S7	0.68	0.68	0.70	0.66	0.65	0.78	0.19
S8	0.72	0.70	0.70	0.65	0.65	0.76	0.25
S9	0.68	0.68	0.63	0.61	0.66	0.70	0.32
S10	0.90	0.85	0.85	0.80	0.85	0.81	0.48
S11	0.59	0.55	0.56	0.48	0.55	0.65	0.12
S12	0.80	0.75	0.71	0.68	0.83	0.88	0.48
S13	0.82	0.76	0.75	0.70	0.88	0.80	0.45
S14	0.78	0.86	0.73	0.78	0.76	0.85	0.48
S15	0.72	0.86	0.76	0.60	0.66	0.63	0.13
Average	**0.74 (±0.07)**	**0.73 (±0.08)**	**0.73 (±0.08)**	**0.70 (±0.09)**	**0.72 (±0.09)**	**0.76 (±0.06)**	**0.38 (±0.15)**

TABLE V
COMPARISON OF DECODING PERFORMANCES BETWEEN THE CONVENTIONAL SPECTRAL FILTERS AND THE PROPOSED SSSF FOR THE PUBLIC DATASET

	Decoding performances (hand open vs. rest)				
Spectral filiter	0.05–5 Hz [37]	0.05–10 Hz [43]	0.1–1 Hz [42]	0.3–3 Hz [50]	SSSF
Grand-average.	**0.48 (±0.05)**	**0.51 (±0.02)**	**0.49 (±0.03)**	**0.50 (±0.09)**	**0.76 (±0.06)**

TABLE VI
STATISTICAL ANALYSIS FOR MULTIPLE COMPARISONS WITH BONFERRONI CORRECTION FOR BOTH OUR DATASET AND THE PUBLIC DATASET

Our dataset			Public dataset		
Groups		*p*-value	Groups		*p*-value
0.05–5 Hz [37]	vs. 0.05–10 Hz [43]	1.000	0.05–5 Hz	vs. 0.05–10 Hz	0.491
0.05–5 Hz	vs. 0.1–1 Hz [42]	0.012	0.05–5 Hz	vs. 0.1–1 Hz	0.696
0.05–5 Hz	vs. 0.3–3 Hz [50]	0.696	0.05–5 Hz	vs. 0.3–3 Hz	0.668
0.05–5 Hz	vs. SSSF	**<0.01**	0.05–5 Hz	vs. SSSF	**<0.01**
0.05–10 Hz	vs. 0.1–1 Hz	0.012	0.05–10 Hz	vs. 0.1–1 Hz	0.282
0.05–10 Hz	vs. 0.3–3 Hz	0.696	0.05–10 Hz	vs. 0.3–3 Hz	0.794
0.05–10 Hz	vs. SSSF	**<0.01**	0.05–10 Hz	vs. SSSF	**<0.01**
0.1–1 Hz	vs. 0.3–3 Hz	0.013	0.1–1 Hz	vs. 0.3–3 Hz	0.413
0.1–1 Hz	vs. SSSF	**<0.01**	0.1–1 Hz	vs. SSSF	**<0.01**
0.3–3 Hz	vs. SSSF	**<0.01**	0.3–3 Hz	vs. SSSF	**<0.01**

Recent brain-computer interface (BCI) studies have also been conducted using various advanced methods such as EEG feature optimization and novel classification algorithms. Zhang et al. [71] developed the spatial-temporal discriminant analysis (STDA). The STDA method maximizes the discriminant information between the target and non-target classes using spatial and temporal dimensions collaboratively. Recently, the authors proposed a sparse Bayesian Laplace priors-based EEG classification method. They adopted a sparse discriminant vector learned using a Laplace prior in a hierarchical manner under a Bayesian evidence framework [72]. In particular, for the MI-BCI to detect user intention, Zhang *et al.* [73] proposed a temporally constrained sparse group spatial pattern (TSGSP) as a novel feature extraction method. The authors evaluated the performance using the public EEG dataset and validated the effectiveness of the proposed TSGSP compared to other competing methods. Shahtalebi and Mohammadi [74] proposed a framework for constructing optimized subject-specific spectral filters in an intuitive fashion resulting in a creation of significantly discriminant features coupled with error-correcting output coding (ECOC) classifiers. Wang and Veluvolu [75] developed a novel method based on an evolutionary algorithm (EA) to optimize the spatial filter in a multiple-channel EEG. Aghaei *et al.* [76] proposed a separable common spatio-spectral pattern (SCSSP) for extracting of discriminant spatio-spectral EEG features in MI-BCI. These advanced methods have contributed to the robust decoding of EEG signals through feature optimization and novel classification depending on the BCI paradigm. Similarly, in this study, we investigated the robust feature selection method and focused on a single-trial MRCP for improving the performance within the endogenous BCI paradigm. The MRCP characteristics can represent a distinct temporal template such as slow negative/positive deflection before and after movement. Therefore, we approached the MRCP components such as RP and MMP section, which can reflect discriminant temporal patterns for feature selection depending on each subject. The SSSF has been verified based on the reliable decoding performance in detecting both walking intention (lower-limb MRCP) and various types of upper extremity intention (upper-limb MRCP).

In addition, in this study, we compared the decoding performance using single-channel and multiple-channels. As the results indicate, the performance showed a slight difference (below 5%) between the multi- and single-channel approaches. This indicates that it may be possible to detect movements using only a single EEG channel for a BMI; hence, it can activate assistive technologies for providing afferent

TABLE VII
COMPUTATIONAL TIME OF PROPOSED SSSF AND BASELINE METHOD BY USING OUR DATASET AND THE PUBLIC DATASET

Elapsed time for our dataset (s)					Elapsed time for public dataset (s)				
Subjects	SSSF		Baseline		Subjects	SSSF		Baseline	
	Training	Test	Training	Test		Training	Test	Training	Test
S1	246.52	0.02	0.73	0.01	S1	4719.90	0.05	5.02	0.06
S2	253.79	0.02	0.35	0.01	S2	4714.50	0.04	4.86	0.04
S3	260.24	0.02	0.28	0.01	S3	4721.80	0.03	5.35	0.06
S4	253.95	0.02	0.26	0.01	S4	6934.12	0.06	5.20	0.06
S5	250.75	0.03	0.30	0.01	S5	6637.05	0.05	5.04	0.04
S6	248.30	0.01	0.24	0.01	S6	5733.01	0.04	4.89	0.04
S7	251.31	0.02	0.33	0.01	S7	5713.94	0.04	4.89	0.04
S8	251.31	0.01	0.36	0.01	S8	5709.94	0.05	4.89	0.05
S9	252.66	0.02	0.43	0.01	S9	5705.24	0.04	4.76	0.04
S10	252.60	0.01	0.37	0.01	S10	5716.10	0.04	4.90	0.04
Average	**252.08**	**0.02**	**0.37**	**0.01**	S11	5701.78	0.04	4.82	0.04
					S12	5710.04	0.04	4.84	0.04
					S13	5734.20	0.04	4.86	0.04
					S14	5710.05	0.04	4.82	0.03
					S15	5824.85	0.05	4.83	0.04
					Average	**5665.77**	**0.04**	**4.93**	**0.04**

feedback [64]. We confirmed that the Cz channel showed a dramatically discriminant performance compared to other nearby channels. As one of the reasons for the Cz channel activation in this study, our experimental data are related to lower-limb movement (i.e., walking). The increased cortical density of each electrode during a body movement is represented throughout the motor cortex according to each body region. The lower limb is closely related within the central location of the motor cortex near the Cz channel [41]. The single-channel BMI approach with optimal sites will lead to the use of a small number of EEG feature vectors for a final decision such that it has potentially reduced the computational time for model training and real-time scenarios.

In addition, we compared the computational time between the proposed SSSF and the baseline method. We measured the elapsed time for model training and testing using the *tic-toc* function in MATLAB software. Table VII shows the computational time required to detect a movement intention when applying our dataset and the public dataset. To validate the elapsed time under the same conditions as much as possible between the proposed and baseline methods, we defined the baseline method as the use of conventional spectral filters. Compared to the SSSF and the baseline method, the averaged training time was 252.08 s and 0.37 s, respectively, whereas the average test times for both methods are 0.01 s when using our dataset. For the public dataset, the training showed average times of 5665.77 s and 4.93 s, respectively, and the test time is 0.04 s. The proposed SSSF method has a critical limitation under a much longer training time than the baseline method. Although the decoding performance is an important challenge, the computational time for model training is also a valuable aspect for adoption in real-world scenarios. Therefore, we plan to modify the SSSF to reduce the model training time. After pre-training the spectral band for the characteristics of the subject using a large MRCP dataset, when new subjects used the SSSF, the computational time for spectral feature selection can be reduced by measuring the probabilistic similarity between the pre-assigned and new subjects, or by applying advanced model optimization methods.

Furthermore, we designed the SSSF based on a subject-dependent approach, which can lead to a dramatic improvement in BMI performance. This strategy considers a large EEG variability between inter-subjects [32], [77]. We adopted a dependent strategy to design the SSSF method and consider the differences in individual MRCP characteristics for each subject. However, under real-world BMI scenarios, one of the ultimate goals is for the BMI system to provide utility and effectiveness for various types of end-users. In particular, MRCP-based BMI technology has been mostly used to rehabilitate the motor functional recovery in patients. One of the important points for a neuro-rehabilitation is to induce the plasticity of brain function through a feedback system; hence, the reliable MRCP performance for user intention decoding is needed. For this reason, a subject-dependent strategy has been adopted, but the long calibration time imposes a high cognitive workload on patients when using a BMI-based neuro-rehabilitation. This problem is a critical point in verifying whether the systems can be adopted in real-world applications. To solve this problem, the proposed SSSF has been modified to consider the subject's common MRCP characteristics and reduce the subject's training time. Fortunately, the MRCP showed a similar amplitude in stroke patients and healthy subjects despite a neural injury, which may be due to better motivation, or the fact that less mental effort and shorter planning are needed [42], [65]. Accordingly, we plan to modify the SSSF to adopt real-world BMI scenarios using a subject-independent approach [78] with short training time.

V. CONCLUSION AND FUTURE WORKS

The robust decoding of a movement intention from EEG signals is an essential and critical issuein the development of self-paced BMI control systems [14]. In this study, we proposed the SSSF method to accurately detect user intentions from an MRCP. The proposed method utilizes two temporal sections, RP (-2 to 0 s) and MMP (0 to 1 s), and the spectral frequencies were selected from each temporal interval. We found that the RP and MMP components have different optimal spectral bands, which are highly dependent on individual subject recordings. Although a direct comparison with previous studies is difficult owing to different experimental protocols and methodologies, a single-trial MRCP detection achieved a high grand-average decoding performance of 0.86 ($\pm$0.09) for all subjects. This result demonstrates the feasibility of BMI-based self-initiated walking with a powered exoskeleton.

Nonetheless, the decoding performance in the pseudo-online analysis remains insufficient for application to real-world BMI scenarios. Furthermore, a critical issue is uncertain external artifacts (e.g., body movements and robot vibrations) under an asynchronous BMI paradigm. In our study, unstable MRCP patterns with large variations were also observed during the exoskeleton running time, despite the use of the FORCe

method. Therefore, to provide stable operating commands, it is necessary to apply the advanced noise reduction algorithms to minimize noise for a real-time environment.

In addition, our experiment data were acquired using only healthy subjects wearing a lower-limb exoskeleton. Therefore, the proposed SSSF should demonstrate the possibility of its application to stroke or paralyzed patients for BMI-based gait rehabilitation. It is more complicated to extract distinctive brain patterns for patients owing to their brain malfunctions. Hence, future work will target an assessment of the robustness of our method among patients to show the possibility of using an MRCP-based exoskeleton system in real-world applications.

ACKNOWLEDGMENT

The authors would like to thank Dr. M.-H. Lee for the useful discussion of the data analysis and for help with EEG data collection.

REFERENCES

[1] T. Vaughan, "Guest editorial brain-computer interface technology: A review of the second international meeting," *IEEE Trans. Neural Syst. Rehabil. Eng.*, vol. 11, no. 2, pp. 94–109, Jun. 2003.

[2] J. Del R. Millan and J. Mourino, "Asynchronous bci and local neural classifiers: An overview of the adaptive brain interface project," *IEEE Trans. Neural Syst. Rehabil. Eng.*, vol. 11, no. 2, pp. 159–161, Jun. 2003.

[3] J. R. Wolpaw, N. Birbaumer, D. J. McFarland, G. Pfurtscheller, and T. M. Vaughan, "Brain–computer interfaces for communication and control," *Clin. Neurophysiol.*, vol. 113, no. 6, pp. 767–791, 2002.

[4] R. Abiri, S. Borhani, E. W. Sellers, Y. Jiang, and X. Zhao, "A comprehensive review of EEG-based brain–computer interface paradigms," *J. Neural Eng.*, vol. 16, no. 1, Feb. 2019, Art. no. 011001.

[5] K.-T. Kim, H.-I. Suk, and S.-W. Lee, "Commanding a brain-controlled wheelchair using steady-state somatosensory evoked potentials," *IEEE Trans. Neural Syst. Rehabil. Eng.*, vol. 26, no. 3, pp. 654–665, Mar. 2018.

[6] L. Cao, J. Li, H. Ji, and C. Jiang, "A hybrid brain computer interface system based on the neurophysiological protocol and brain-actuated switch for wheelchair control," *J. Neuroscience Methods*, vol. 229, pp. 33–43, May 2014.

[7] C. I. Penaloza and S. Nishio, "BMI control of a third arm for multitasking," *Sci. Robot.*, vol. 3, no. 20, Jul. 2018, Art. no. eaat1228.

[8] J.-H. Jeong, K.-H. Shim, D.-J. Kim, and S.-W. Lee, "Trajectory decoding of arm reaching movement imageries for brain-controlled robot arm system," in *Proc. 41st Annu. Int. Conf. IEEE Eng. Med. Biol. Soc. (EMBC)*, Berlin, Germany, Jul. 2019, pp. 5544–5547.

[9] J.-H. Kim, F. Biessmann, and S.-W. Lee, "Decoding three-dimensional trajectory of executed and imagined arm movements from electroencephalogram signals," *IEEE Trans. Neural Syst. Rehabil. Eng.*, vol. 23, no. 5, pp. 867–876, Sep. 2015.

[10] J. Meng, S. Zhang, A. Bekyo, J. Olsoe, B. Baxter, and B. He, "Non-invasive electroencephalogram based control of a robotic arm for reach and grasp tasks," *Sci. Rep.*, vol. 6, Dec. 2016, Art. no. 38565.

[11] A. H. Do, P. T. Wang, C. E. King, S. N. Chun, and Z. Nenadic, "Brain-computer interface controlled robotic gait orthosis," *J. NeuroEng. Rehabil.*, vol. 10, no. 1, p. 111, 2013.

[12] N.-S. Kwak, K.-R. Müller, and S.-W. Lee, "A lower limb exoskeleton control system based on steady state visual evoked potentials," *J. Neural Eng.*, vol. 12, no. 5, Oct. 2015, Art. no. 056009.

[13] J. L. Contreras-Vidal *et al.*, "Powered exoskeletons for bipedal locomotion after spinal cord injury," *J. Neural Eng.*, vol. 13, no. 3, Jun. 2016, Art. no. 031001.

[14] Y. He, D. Eguren, J. M. Azorín, R. G. Grossman, T. P. Luu, and J. L. Contreras-Vidal, "Brain-machine interfaces for controlling lower-limb powered robotic systems," *J. Neural Eng.*, vol. 15, no. 2, Apr. 2018, Art. no. 021004.

[15] I.-H. Kim, J.-W. Kim, S. Haufe, and S.-W. Lee, "Detection of braking intention in diverse situations during simulated driving based on EEG feature combination," *J. Neural Eng.*, vol. 12, no. 1, Feb. 2015, Art. no. 016001.

[16] S.-K. Yeom, S. Fazli, K.-R. Müller, and S.-W. Lee, "An efficient ERP-based brain-computer interface using random set presentation and face familiarity," *PLoS ONE*, vol. 9, no. 11, Nov. 2014, Art. no. e111157.

[17] Y. Zhang, S. Prasad, A. Kilicarslan, and J. L. Contreras-Vidal, "Multiple kernel based region importance learning for neural classification of gait states from EEG signals," *Frontiers Neurosci.*, vol. 11, p. 170, Apr. 2017.

[18] K. K. Ang and C. Guan, "EEG-based strategies to detect motor imagery for control and rehabilitation," *IEEE Trans. Neural Syst. Rehabil. Eng.*, vol. 25, no. 4, pp. 392–401, Apr. 2017.

[19] K. Gui, H. Liu, and D. Zhang, "Toward multimodal human–robot interaction to enhance active participation of users in gait rehabilitation," *IEEE Trans. Neural Syst. Rehabil. Eng.*, vol. 25, no. 11, pp. 2054–2066, Nov. 2017.

[20] M. Lee *et al.*, "Motor imagery learning across a sequence of trials in stroke patients," *Restor. Neurol. Neurosci.*, vol. 34, no. 4, pp. 635–645, Aug. 2016.

[21] T.-E. Kam, H.-I. Suk, and S.-W. Lee, "Non-homogeneous spatial filter optimization for ElectroEncephaloGram (EEG)-based motor imagery classification," *Neurocomputing*, vol. 108, pp. 58–68, May 2013.

[22] S. K. Goh *et al.*, "spatio–spectral representation learning for electroencephalographic gait-pattern classification," *IEEE Trans. Neural Syst. Rehabil. Eng.*, vol. 26, no. 9, pp. 1858–1867, Sep. 2018.

[23] A. Úbeda, J. M. Azorín, R. Chavarriaga, and J. D. R. Millán, "Classification of upper limb center-out reaching tasks by means of EEG-based continuous decoding techniques," *J. Neuroeng. Rehabil.*, vol. 14, no. 1, p. 9, 2017.

[24] R. Salazar-Varas, A. Costa, E. Iáñez, A. Úbeda, E. Hortal, and J. Azorín, "Analyzing EEG signals to detect unexpected obstacles during walking," *J. Neuroeng. Rehabil.*, vol. 12, no. 1, p. 101, 2015.

[25] H. Yang, K. Ang, C. Wang, K. Phua, and C. Guan, "Neural and cortical analysis of swallowing and detection of motor imagery of swallow for dysphagia rehabilitation—A review," *Prog. Brain Res.*, vol. 228, pp. 185–219, Jun. 2016.

[26] N.-S. Kwak, K.-R. Müller, and S.-W. Lee, "A convolutional neural network for steady state visual evoked potential classification under ambulatory environment," *PLoS ONE*, vol. 12, no. 2, Feb. 2017, Art. no. e0172578.

[27] J.-H. Jeong, M.-H. Lee, N.-S. Kwak, and S.-W. Lee, "Single-trial analysis of readiness potentials for lower limb exoskeleton control," in *Proc. 5th Int. Winter Conf. Brain-Comput. Interface (BCI)*, Jan. 2017, pp. 50–52.

[28] L. Yao, N. Mrachacz-Kersting, X. Sheng, X. Zhu, D. Farina, and N. Jiang, "A multi-class BCI based on somatosensory imagery," *IEEE Trans. Neural Syst. Rehabil. Eng.*, vol. 26, no. 8, pp. 1508–1515, Aug. 2018.

[29] N. Tang, C. Guan, K. Ang, K. Phua, and E. Chew, "Motor imagery-assisted brain-computer interface for gait retraining in neurorehabilitation in chronic stroke," *Ann. Phys. Rehabil. Med.*, vol. 61, p. e188, Jul. 2018.

[30] M. Jochumsen, I. K. Niazi, R. W. Nedergaard, M. S. Navid, and K. Dremstrup, "Effect of subject training on a movement-related cortical potential-based brain-computer interface," *Biomed. Signal Process. Control*, vol. 41, pp. 63–68, Mar. 2018.

[31] H. Yang, C. Guan, C. C. Wang, and K. K. Ang, "Detection of motor imagery of brisk walking from electroencephalogram," *J. Neurosci. Methods*, vol. 244, pp. 33–44, Apr. 2015.

[32] H.-I. Suk and S.-W. Lee, "A novel Bayesian framework for discriminative feature extraction in brain-computer interfaces," *IEEE Trans. Pattern Anal. Mach. Intell.*, vol. 35, no. 2, pp. 286–299, Feb. 2013.

[33] H. Shibasaki and M. Hallett, "What is the Bereitschaftspotential?" *Clin. Neurophysiol.*, vol. 117, no. 11, pp. 2341–2356, Nov. 2006.

[34] A. Shakeel *et al.*, "A review of techniques for detection of movement intention using movement-related cortical potentials," *Comput. Math. Method*, vol. 2015, Dec. 2015, Art. no. 346217.

[35] J. Liu, M. Abd-El-Barr, and J. H. Chi, "Long-term training with a brain-machine interface-based gait protocol induces partial neurological recovery in paraplegic patients," *Neurosurgery*, vol. 79, no. 6, pp. N13–N14, Dec. 2016.

[36] J.-H. Jeong, K.-T. Kim, D.-J. Kim, and S.-W. Lee, "Decoding of Multi-directional Reaching Movements for EEG-Based Robot Arm Control," in *Proc. IEEE Int. Conf. Syst., Man, (SMC)*, Oct. 2018, pp. 511–514.

[37] M. Jochumsen *et al.*, "Quantification of movement-related eeg correlates associated with motor training: A study on movement-related cortical potentials and sensorimotor rhythms," *Frontiers Hum. Neurosci.*, vol. 11, p. 604, Dec. 2017.

[38] A. Schwarz, P. Ofner, J. Pereira, A. I. Sburlea, and G. R. Müller-Putz, "Decoding natural reach-and-grasp actions from human EEG," *J. Neural Eng.*, vol. 15, no. 1, Feb. 2018, Art. no. 016005.

[39] T. C. Bulea, S. Prasad, A. Kilicarslan, and J. L. Contreras-Vidal, "Sitting and standing intention can be decoded from scalp EEG recorded prior to movement execution," *Frontiers Neurosci.*, vol. 8, no. 376, pp. 1–19, 2014.

[40] M. Schultze-Kraft *et al.*, "The point of no return in vetoing self-initiated movements," *Proc. Nat. Acad. Sci. USA*, vol. 113, no. 4, pp. 1080–1085, Jan. 2016.

[41] P. Ahmadian, S. Sanei, L. Ascari, L. Gonzalez-Villanueva, and M. A. Umilta, "Constrained blind source extraction of readiness potentials from EEG," *IEEE Trans. Neural Syst. Rehabil. Eng.*, vol. 21, no. 4, pp. 567–575, Jul. 2013.

[42] D. Liu *et al.*, "EEG-based lower-limb movement onset decoding: Continuous classification and asynchronous detection," *IEEE Trans. Neural Syst. Rehabil. Eng.*, vol. 26, no. 8, pp. 1626–1635, Aug. 2018.

[43] C. Lin, B.-H. Wang, N. Jiang, R. Xu, N. Mrachacz-Kersting, and D. Farina, "Discriminative manifold learning based detection of movement-related cortical potentials," *IEEE Trans. Neural Syst. Rehabil. Eng.*, vol. 24, no. 9, pp. 921–927, Mar. 2016.

[44] M. Jochumsen, I. K. Niazi, N. Mrachacz-Kersting, N. Jiang, D. Farina, and K. Dremstrup, "Comparison of spatial filters and features for the detection and classification of movement-related cortical potentials in healthy individuals and stroke patients," *J. Neural Eng.*, vol. 12, no. 5, Oct. 2015, Art. no. 056003.

[45] K. Lee, D. Liu, L. Perroud, R. Chavarriaga, and J. D. R. Millán, "A brain-controlled exoskeleton with cascaded event-related desynchronization classifiers," *Robot. Auto. Syst.*, vol. 90, pp. 15–23, Apr. 2017.

[46] A. I. Sburlea, L. Montesano, and J. Minguez, "Continuous detection of the self-initiated walking pre-movement state from EEG correlates without session-to-session recalibration," *J. Neural Eng.*, vol. 12, no. 3, Jun. 2015, Art. no. 036007.

[47] G. Lisi and J. Morimoto, "EEG single-trial detection of gait speed changes during treadmill walk," *PLoS ONE*, vol. 10, no. 5, May 2015, Art. no. e0125479.

[48] G. Garipelli, R. Chavarriaga, and J. Del R Millán, "Single trial analysis of slow cortical potentials: A study on anticipation related potentials," *J. Neural Eng.*, vol. 10, no. 3, Jun. 2013, Art. no. 036014.

[49] I. K. Niazi, N. Jiang, O. Tiberghien, J. F. Nielsen, K. Dremstrup, and D. Farina, "Detection of movement intention from single-trial movement-related cortical potentials," *J. Neural Eng.*, vol. 8, no. 6, Oct. 2011, Art. no. 066009.

[50] P. Ofner, A. Schwarz, J. Pereira, and G. R. Müller-Putz, "Upper limb movements can be decoded from the time-domain of low-frequency EEG," *PLoS ONE*, vol. 12, no. 8, Aug. 2017, Art. no. e0182578.

[51] R. Xu, N. Jiang, C. Lin, N. Mrachacz-Kersting, K. Dremstrup, and D. Farina, "Enhanced low-latency detection of motor intention from eeg for closed-loop brain-computer interface applications," *IEEE Trans. Biomed. Eng.*, vol. 61, no. 2, pp. 288–296, Feb. 2014.

[52] N. Jiang, L. Gizzi, N. Mrachacz-Kersting, K. Dremstrup, and D. Farina, "A brain-computer interface for single-trial detection of gait initiation from movement related cortical potentials," *Clin. Neurophysiol.*, vol. 126, no. 1, pp. 154–159, Jan. 2015.

[53] H. Li *et al.*, "Combining movement-related cortical potentials and event-related desynchronization to study movement preparation and execution," *Front. Neurol.*, vol. 9, no. 822, pp. 1–11, 2018.

[54] J. Ibáñez *et al.*, "Detection of the onset of upper-limb movements based on the combined analysis of changes in the sensorimotor rhythms and slow cortical potentials," *J. Neural Eng.*, vol. 11, no. 5, Oct. 2014, Art. no. 056009.

[55] U. Rashid, I. K. Niazi, M. Jochumsen, L. R. Krol, N. Signal, and D. Taylor, "Automated labeling of movement- related cortical potentials using segmented regression," *IEEE Trans. Neural Syst. Rehabil. Eng.*, vol. 27, no. 6, pp. 1282–1291, Jun. 2019.

[56] A. I. Sburlea, L. Montesano, and J. Minguez, "Advantages of EEG phase patterns for the detection of gait intention in healthy and stroke subjects," *J. Neural Eng.*, vol. 14, no. 3, Jun. 2017, Art. no. 036004.

[57] N. A. Bhagat *et al.*, "Design and optimization of an EEG-based brain machine interface (BMI) to an upper-limb exoskeleton for stroke survivors," *Frontiers Neurosci.*, vol. 10, no. 122, pp. 1–17, 2016.

[58] M. Jochumsen, I. K. Niazi, M. S. Navid, M. N. Anwar, D. Farina, and K. Dremstrup, "Online multi-class brain-computer interface for detection and classification of lower limb movement intentions and kinetics for stroke rehabilitation," *Brain-Comput. Inter.*, vol. 2, no. 4, pp. 202–210, Oct. 2015.

[59] F. Karimi, J. Kofman, N. Mrachacz-Kersting, D. Farina, and N. Jiang, "Detection of movement related cortical potentials from EEG using constrained ICA for brain-computer interface applications," *Frontiers Neurosci.*, vol. 11, p. 356, Jun. 2017.

[60] G. Staude and W. Wolf, "Objective motor response onset detection in surface myoelectric signals," *Med. Eng. Phys.*, vol. 21, nos. 6–7, pp. 449–467, Jul. 1999.

[61] B. Blankertz *et al.*, "The Berlin brain–computer interface: Non-medical uses of BCI technology," *Frontiers Neurosci.*, vol. 4, no. 3, pp. 1–13, Dec. 2010.

[62] M.-H. Lee *et al.*, "EEG dataset and openbmi toolbox for three BCI paradigms: An investigation into BCI illiteracy," *GigaScience*, vol. 8, no. 5, 2019, Art. no. giz002.

[63] C. Guger, B. Z. Allison, and N. Mrachacz-Kersting, "Brain-computer interface research: A state-of-the-art summary 7," in *Brain-Computer Interface Research* (SpringerBriefs in Electrical and Computer Engineering). Cham, Switzerland: Springer, 2019, pp. 1–9.

[64] A. Delorme and S. Makeig, "EEGLAB: An open source toolbox for analysis of single-trial EEG dynamics including independent component analysis," *J. Neurosci. Methods*, vol. 134, no. 1, pp. 9–21, Mar. 2004.

[65] M. Jochumsen, I. Khan Niazi, D. Taylor, D. Farina, and K. Dremstrup, "Detecting and classifying movement-related cortical potentials associated with hand movements in healthy subjects and stroke patients from single-electrode, single-trial EEG," *J. Neural Eng.*, vol. 12, no. 5, Oct. 2015, Art. no. 056013.

[66] B. Blankertz, S. Lemm, M. Treder, S. Haufe, and K.-R. Müller, "Single-trial analysis and classification of ERP components—A tutorial," *Neuroimage*, vol. 56, no. 2, pp. 814–825, May 2011.

[67] M. S. Treder, A. K. Porbadnigk, F. Shahbazi Avarvand, K.-R. Müller, and B. Blankertz, "The LDA beamformer: Optimal estimation of ERP source time series using linear discriminant analysis," *NeuroImage*, vol. 129, pp. 279–291, Apr. 2016.

[68] B. Blankertz, G. Curio, and K.-R. Müller, "Classifying single trial EEG: Towards brain computer interfacing," in *Proc. Adv. Neural Inf. Process. Syst.*, Dec. 2002, pp. 157–164.

[69] M.-H. Lee, S. Fazli, J. Mehnert, and S.-W. Lee, "Subject-dependent classification for robust idle state detection using multi-modal neuroimaging and data-fusion techniques in BCI," *Pattern Recognit.*, vol. 48, no. 8, pp. 2725–2737, Aug. 2015.

[70] I. Daly, R. Scherer, M. Billinger, and G. Muller-Putz, "FORCe: Fully Online and automated artifact removal for brain-computer interfacing," *IEEE Trans. Neural Syst. Rehabil. Eng.*, vol. 23, no. 5, pp. 725–736, Sep. 2015.

[71] Y. Zhang, G. Zhou, Q. Zhao, J. Jin, X. Wang, and A. Cichocki, "Spatial-temporal discriminant analysis for ERP-based brain-computer interface," *IEEE Trans. Neural Syst. Rehabil. Eng.*, vol. 21, no. 2, pp. 233–243, Mar. 2013.

[72] Y. Zhang, G. Zhou, J. Jin, Q. Zhao, X. Wang, and A. Cichocki, "Sparse Bayesian classification of EEG for brain–computer interface," *IEEE Trans. Neural Netw. Learn. Syst.*, vol. 27, no. 11, pp. 2256–2267, Nov. 2016.

[73] Y. Zhang, C. S. Nam, G. Zhou, J. Jin, X. Wang, and A. Cichocki, "Temporally constrained sparse group spatial patterns for motor imagery BCI," *IEEE Trans. Cybern.*, vol. 49, no. 9, pp. 3322–3332, Sep. 2019.

[74] S. Shahtalebi and A. Mohammadi, "Bayesian optimized spectral filters coupled with ternary ecoc for single-trial eeg classification," *IEEE Trans. Neural Syst. Rehabil. Eng.*, vol. 26, no. 12, pp. 2249–2259, Dec. 2018.

[75] Y. Wang and K. C. Veluvolu, "Evolutionary algorithm based feature optimization for multi-channel EEG classification," *Front. Neurosci.*, vol. 11, p. 28, Feb. 2017.

[76] A. S. Aghaei, M. S. Mahanta, and K. N. Plataniotis, "Separable common spatio-spectral patterns for motor imagery BCI systems," *IEEE Trans. Biomed. Eng.*, vol. 63, no. 1, pp. 15–29, Jan. 2016.

[77] N.-S. Kwak and S.-W. Lee, "Error correction regression framework for enhancing the decoding accuracies of ear-EEG brain-computer interfaces," *IEEE Trans. Cybern.*, to be published.

[78] O.-Y. Kwon, M.-H. Lee, C. Guan, and S.-W. Lee, "Subject-independent brain-computer interfaces based on deep convolutional neural networks," *IEEE Trans. Neural Netw. Learn. Syst.*, to be published.